Supporting information

Covalently fluorophore functionalized ZIF-8 colloidal particles as a sensing platform for endocrine disrupting chemicals such as phthalates plasticizers

Ander Chapartegui-Arias[a,b], Jose A. Villajos[a], Anett Myxa[a], Sebastian Beyer[a,c], Jana Falkenhagen[a], Rudolf J. Schneider[a,d], Franziska Emmerling*[a].

[a]Federal Institute for Materials Research and Testing (BAM), Richard-Willstätter- Str. 11, D – 12489 Berlin, Germany.
[b]Department of Chemistry, Humboldt-Universität zu Berlin, Brook-Taylor-Str. 2, D – 12489 Berlin, Germany.
[c]Chinese University of Hong Kong, Institute for Tissue Engineering and Regenerative Medicine, Shatin, Hong Kong
[d]Technische Universität Berlin, Straße des 17. Juni 135, D – 10623 Berlin, Germany..

Correspondence should be addressed to:

Dr. Franziska Emmerling
BAM Federal Institute for Materials Research and Testing
Richard-Willstätter- Str. 11, D – 12489 Berlin, Germany
Email: franzisca.emmerling@bam.de
Tel: +493081041133

On the following document we provide the necessary information to complement the discussion provided on the associated paper. It is divided in five parts: i) Structural characterization of the modified ZIFs via powder x-ray diffraction; ii) Particle size distribution characterization via electron microscopy; iii) Composition determination of the modified ZIFs via HPLC (after digestion); iiii) photophysical characterization of the modified ZIFs; v) Pore size distribution studies for the obtained ZIFs.

i) Structural Characterization of the modified ZIFs via x-ray diffraction

Powder x-ray diffractograms

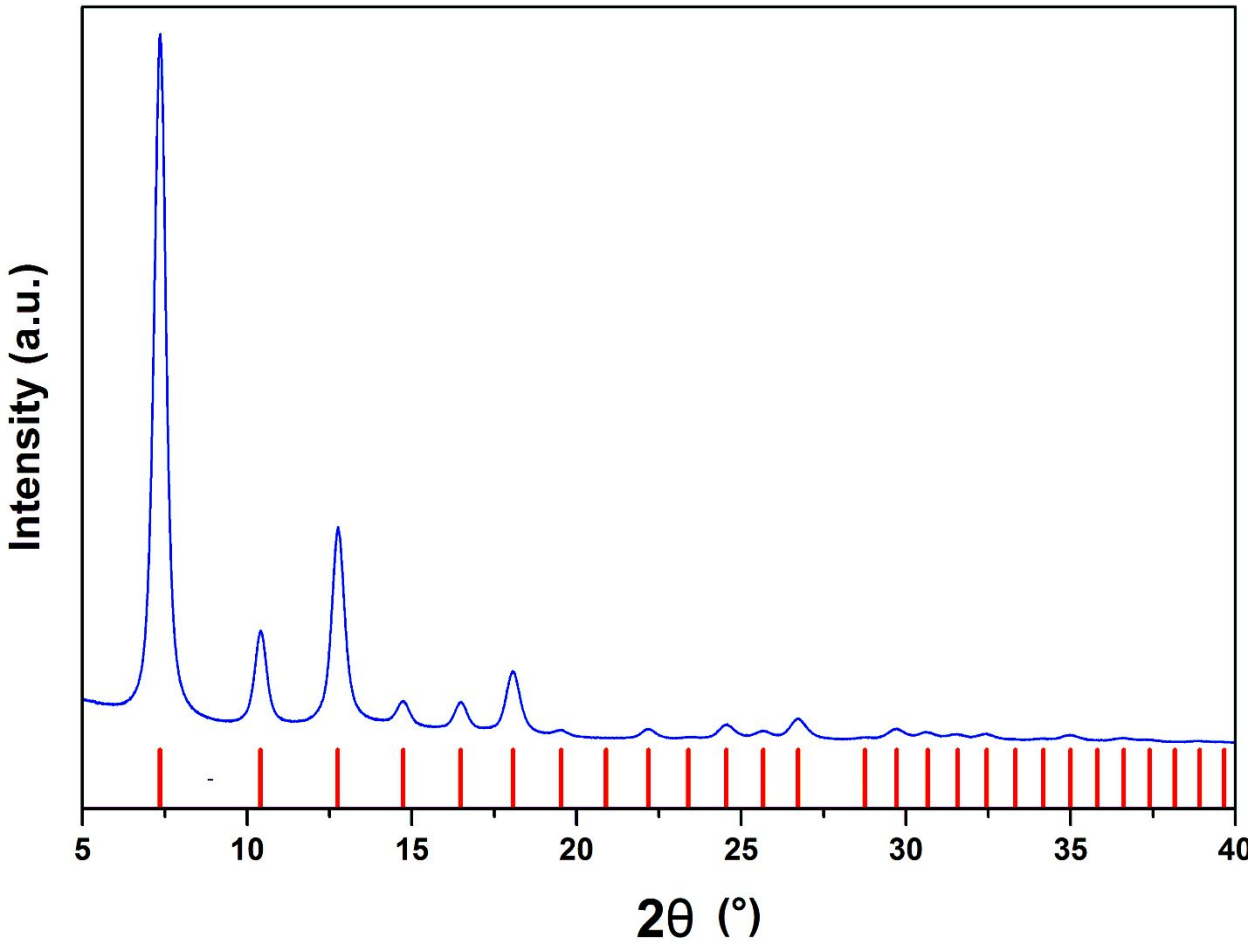

Figure S1_a. Powder X-Ray diffractogram for Z8P-0.25

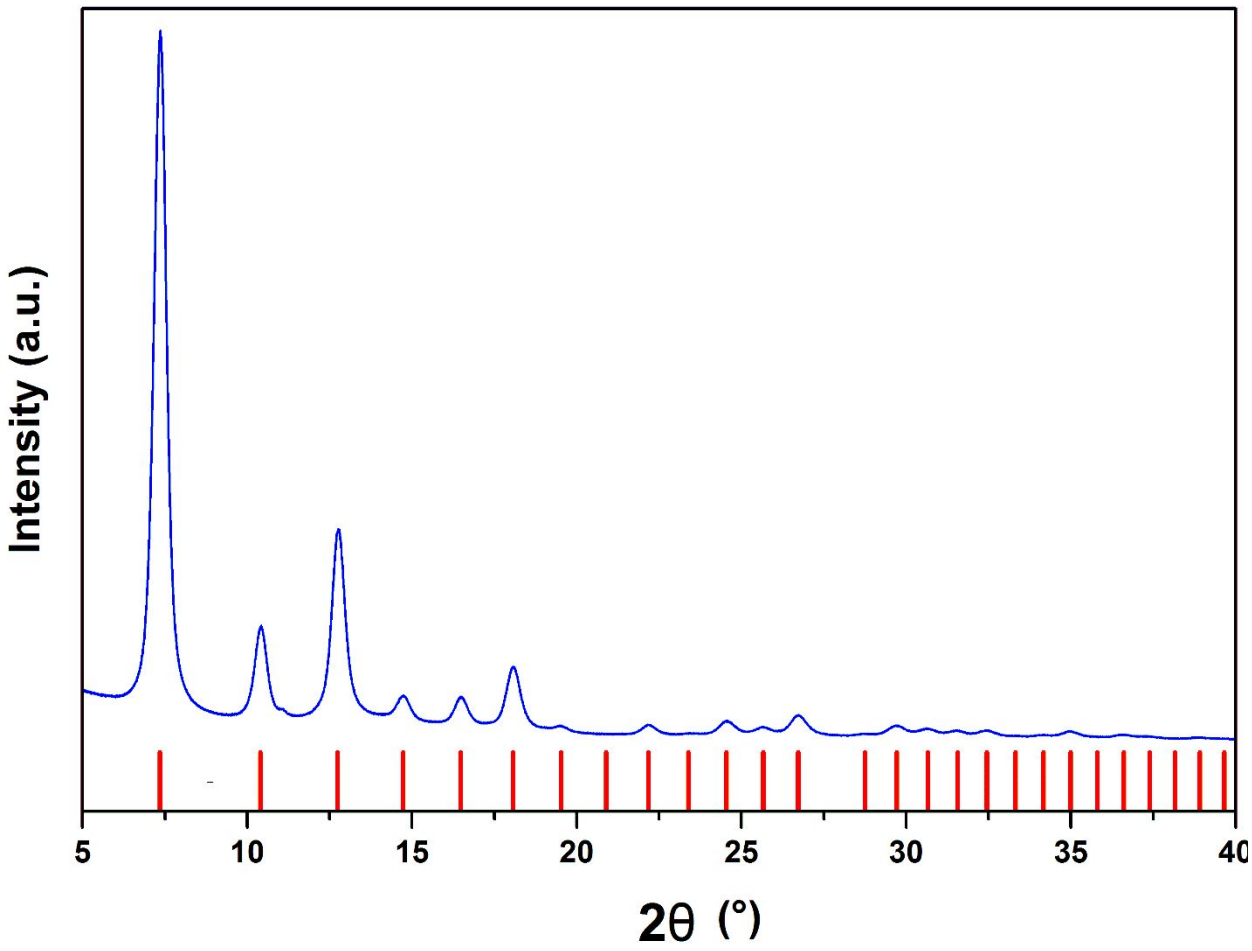

Figure S1_b. Powder X-Ray diffractogram for Z8P-0.50

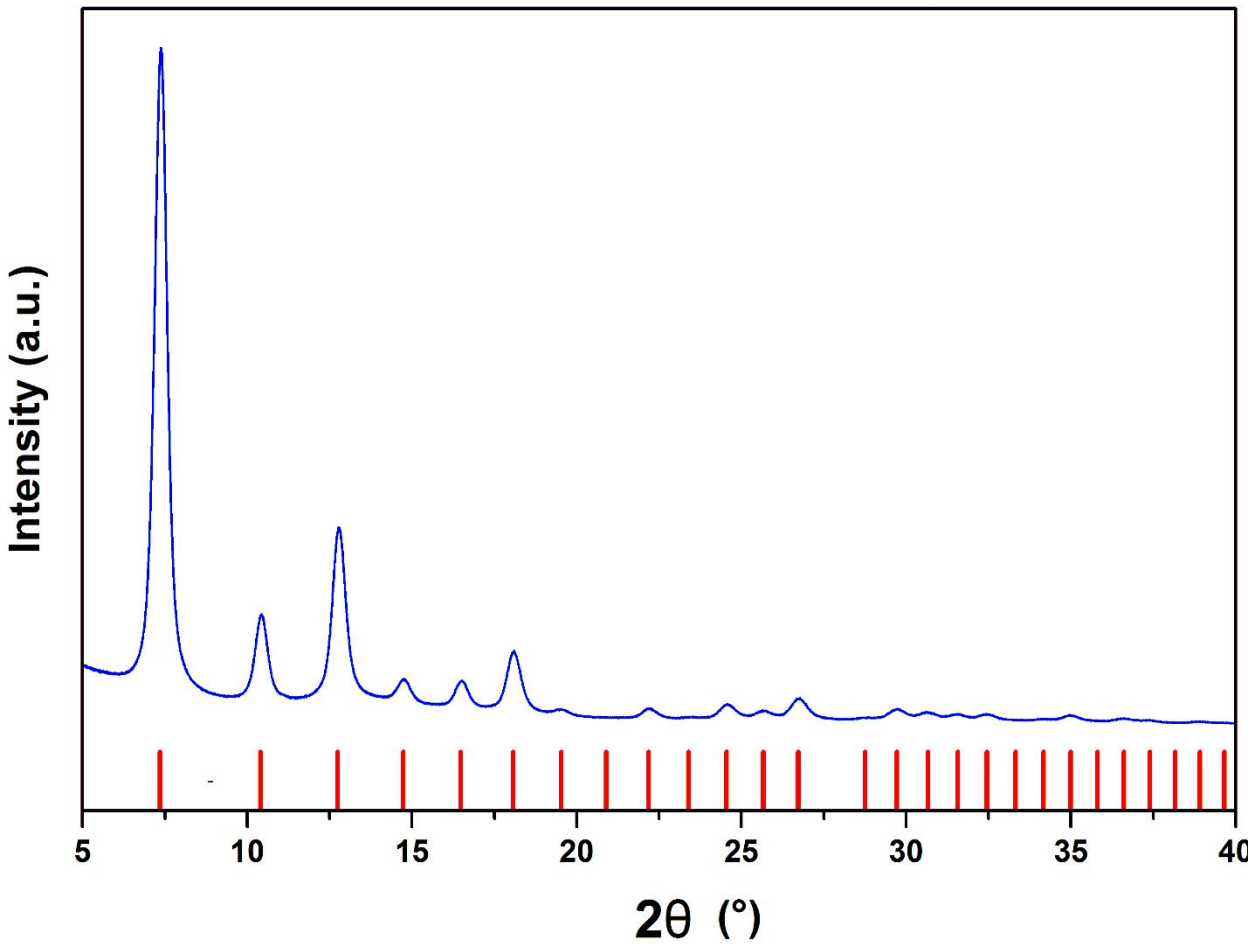

Figure S1_c. Powder X-Ray diffractogram for Z8P-0.75

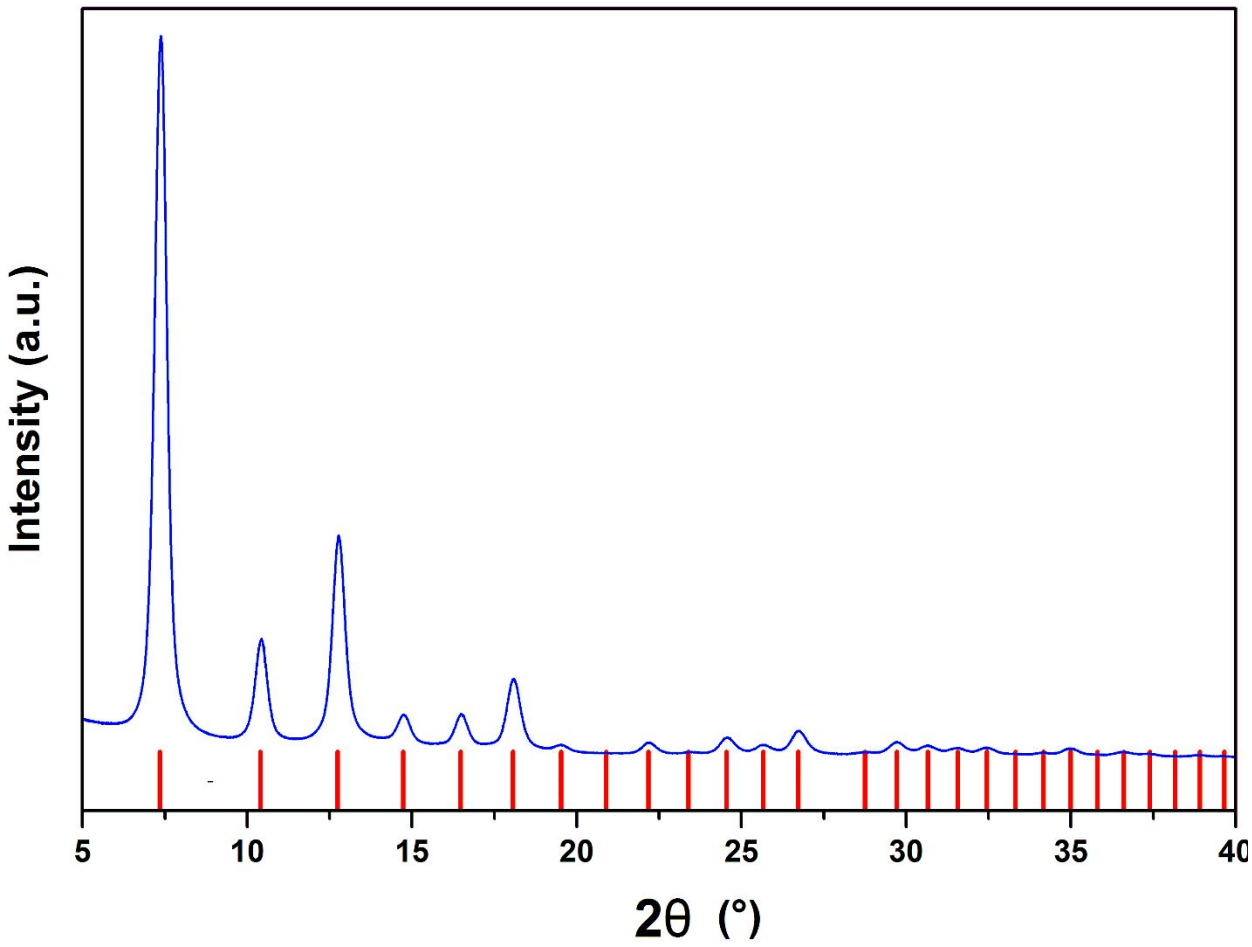

Figure S1_d. Powder X-Ray diffractogram for Z8P-1.00

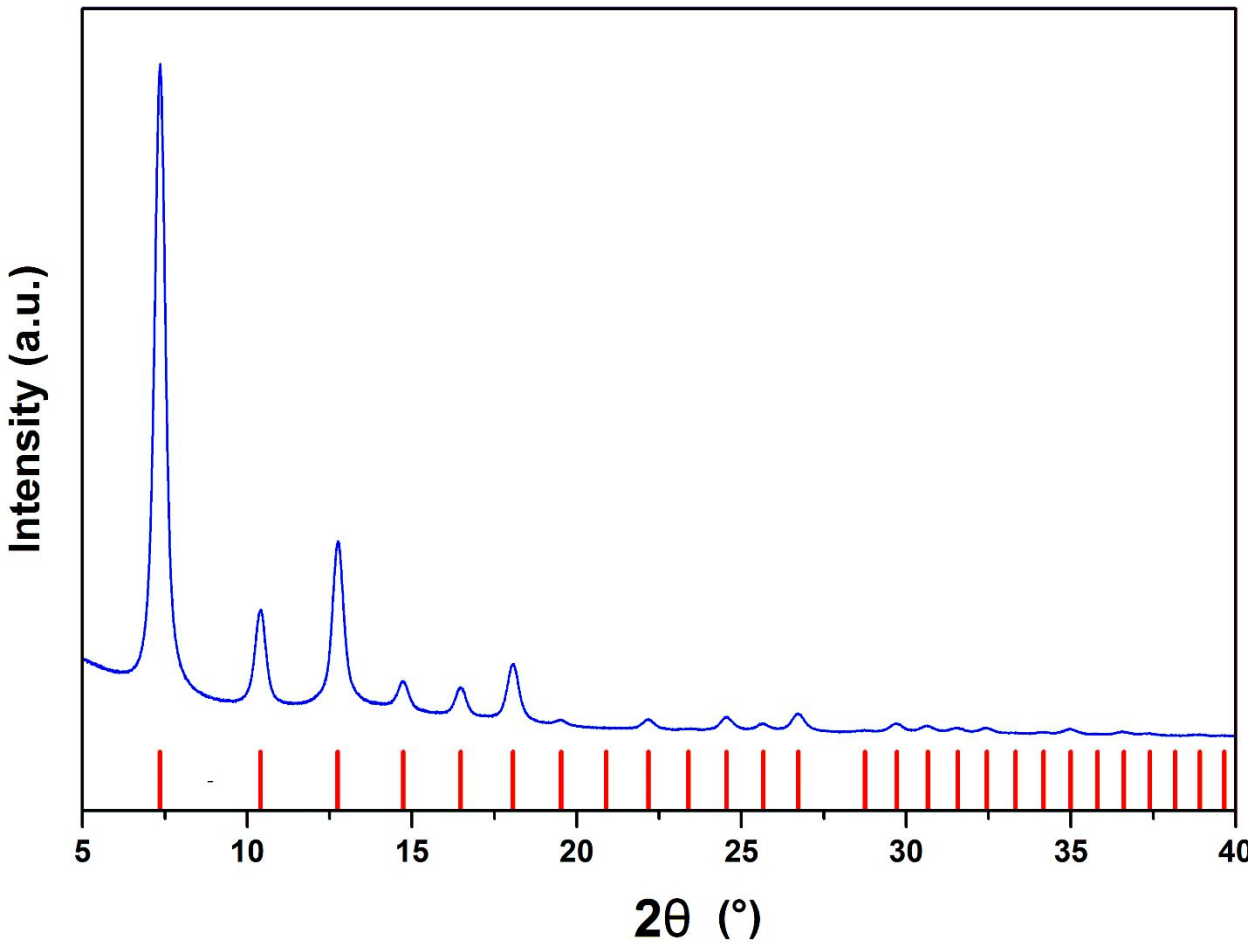

Figure S1_e. Powder X-Ray diffractogram for Z8P-2.50

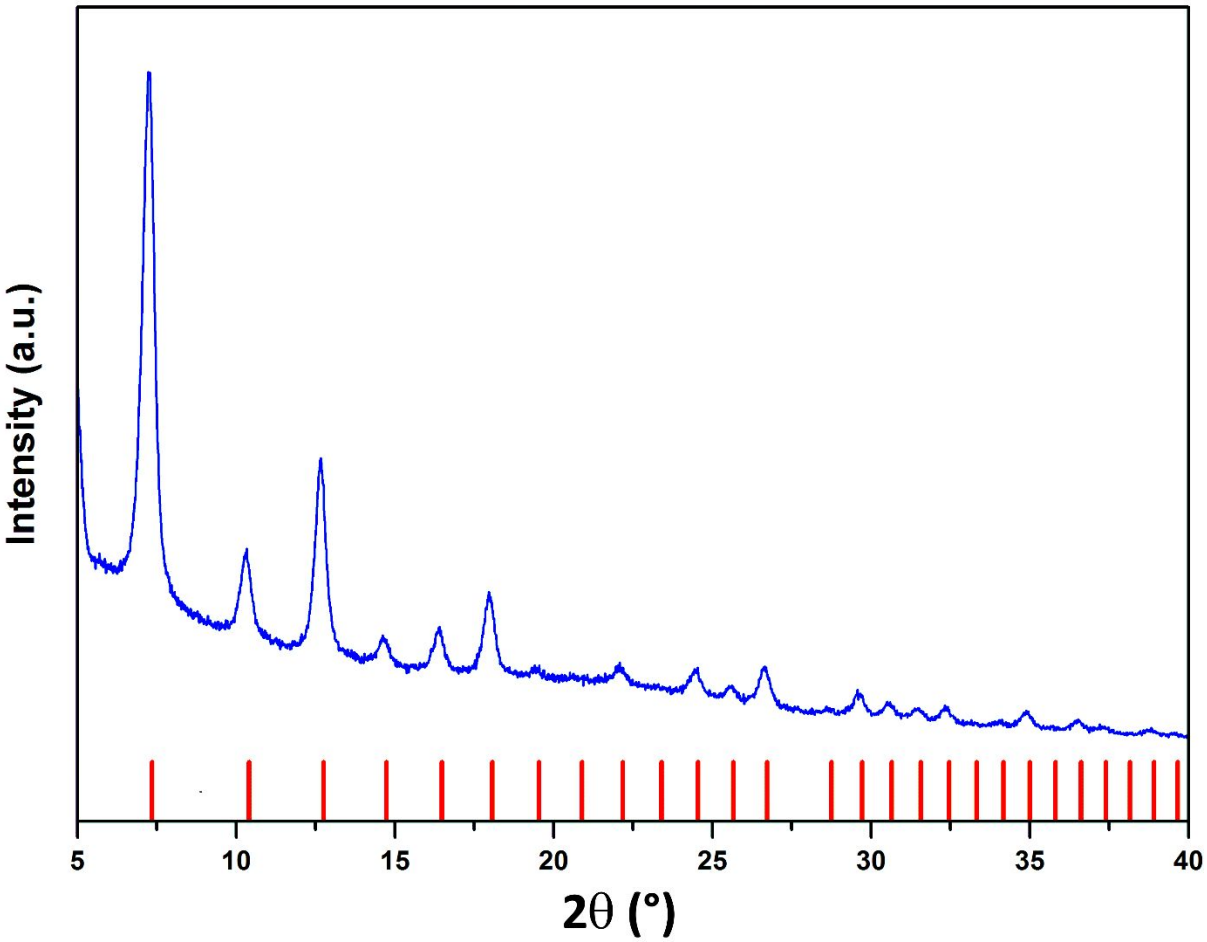

Figure S1_f. Powder X-Ray diffractogram for the nanoparticulated ZIF-8

ii) Particle size and size distribution characterization of the modified ZIFs via Transmission Electron Microscopy

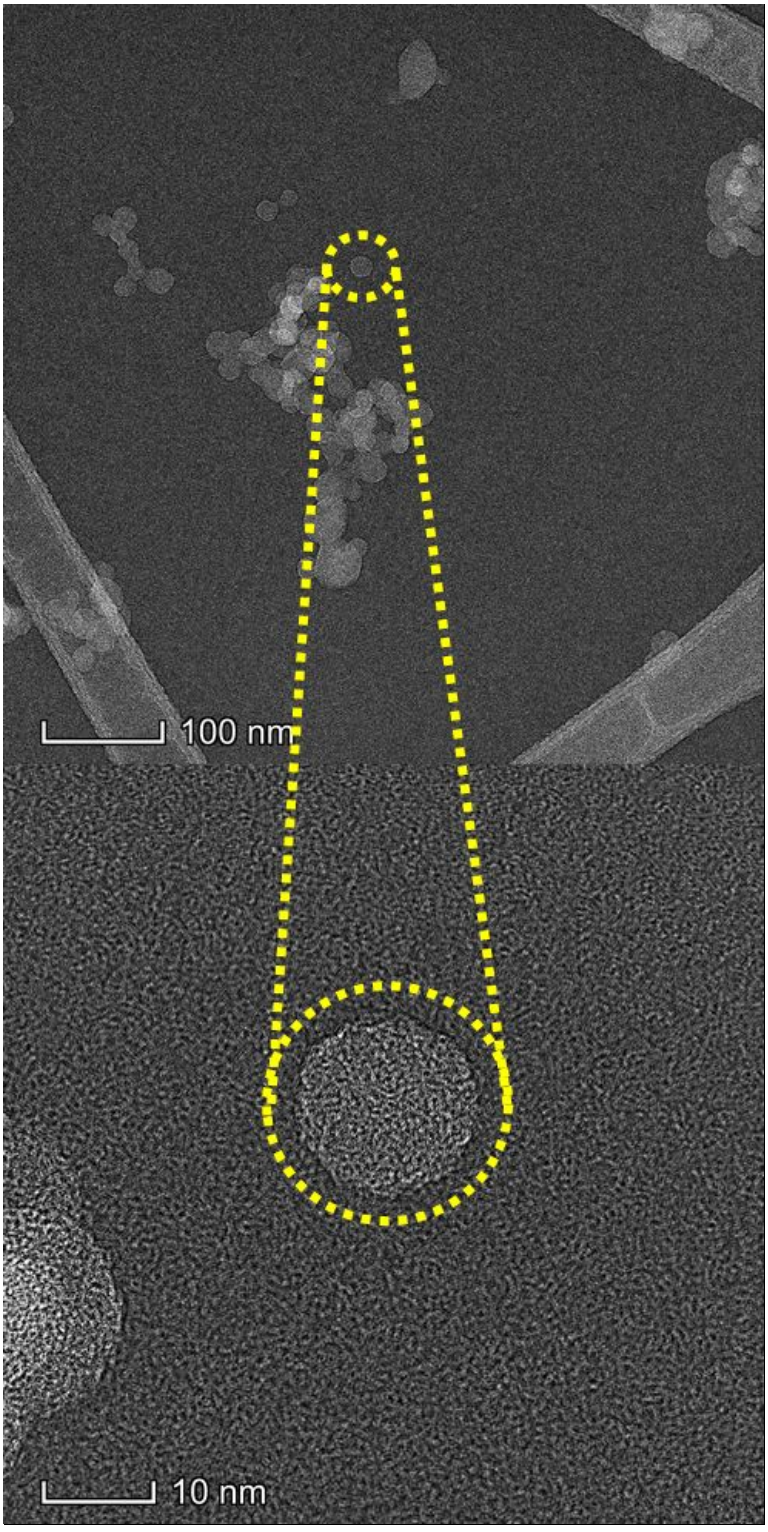

Figure S2_a. TEM Image for Z8P-5.00 nanoparticles.

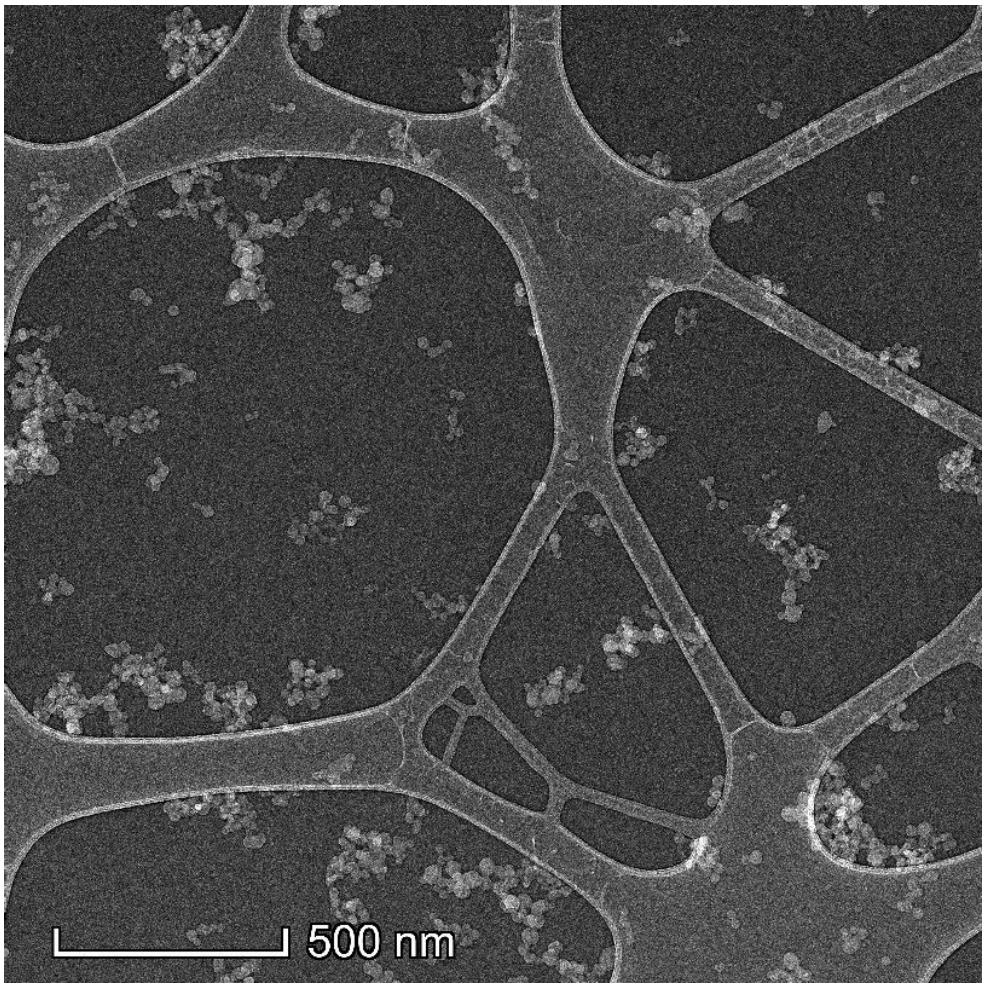

Figure S2_b. Overview of Z8P-5.00 particles

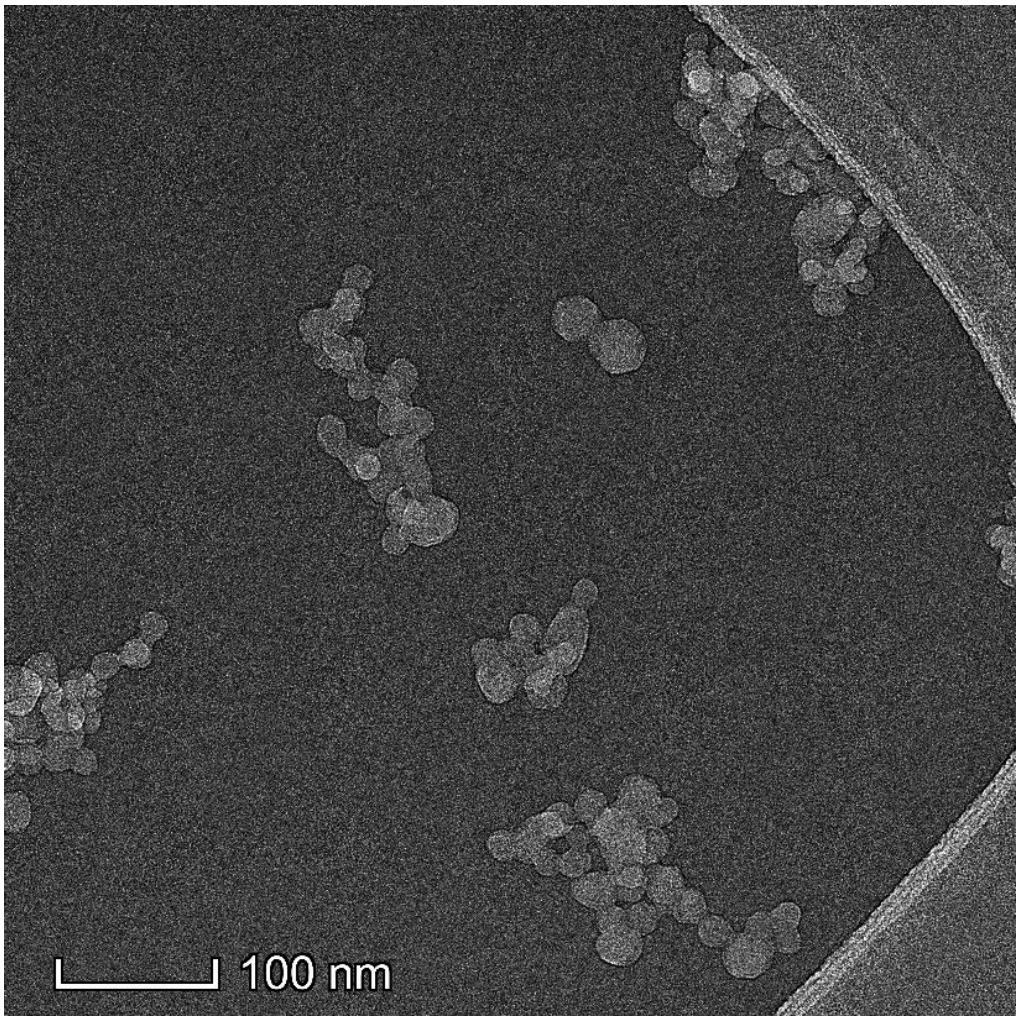

Figure S2_c. Overview of Z8P-5.00 particles

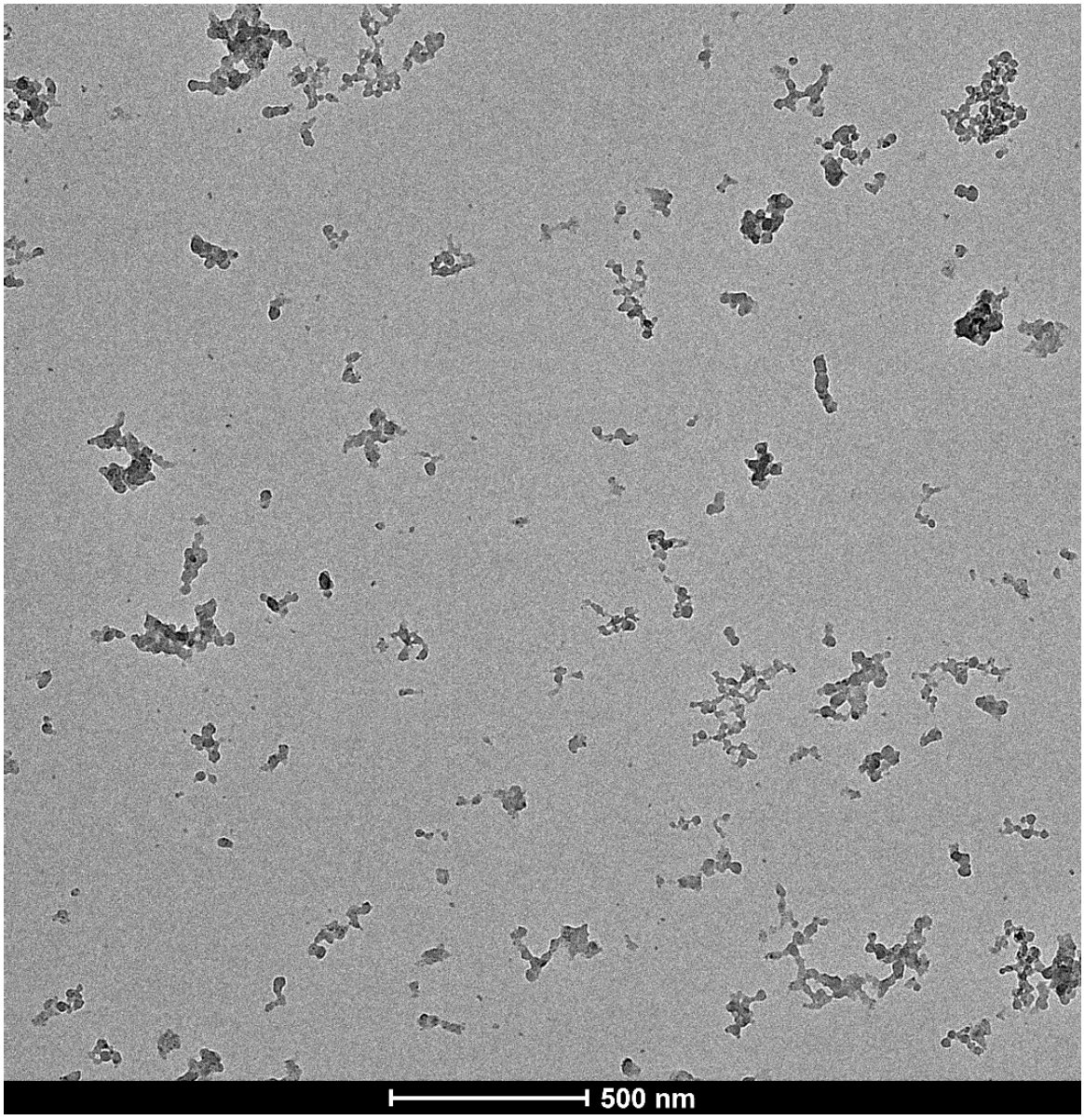

Figure S2_d. Overview of Z8P-0.50 particles

iii) Composition determination of the modified ZIFs via HPLC (after digestion

HPLC Chromatograms

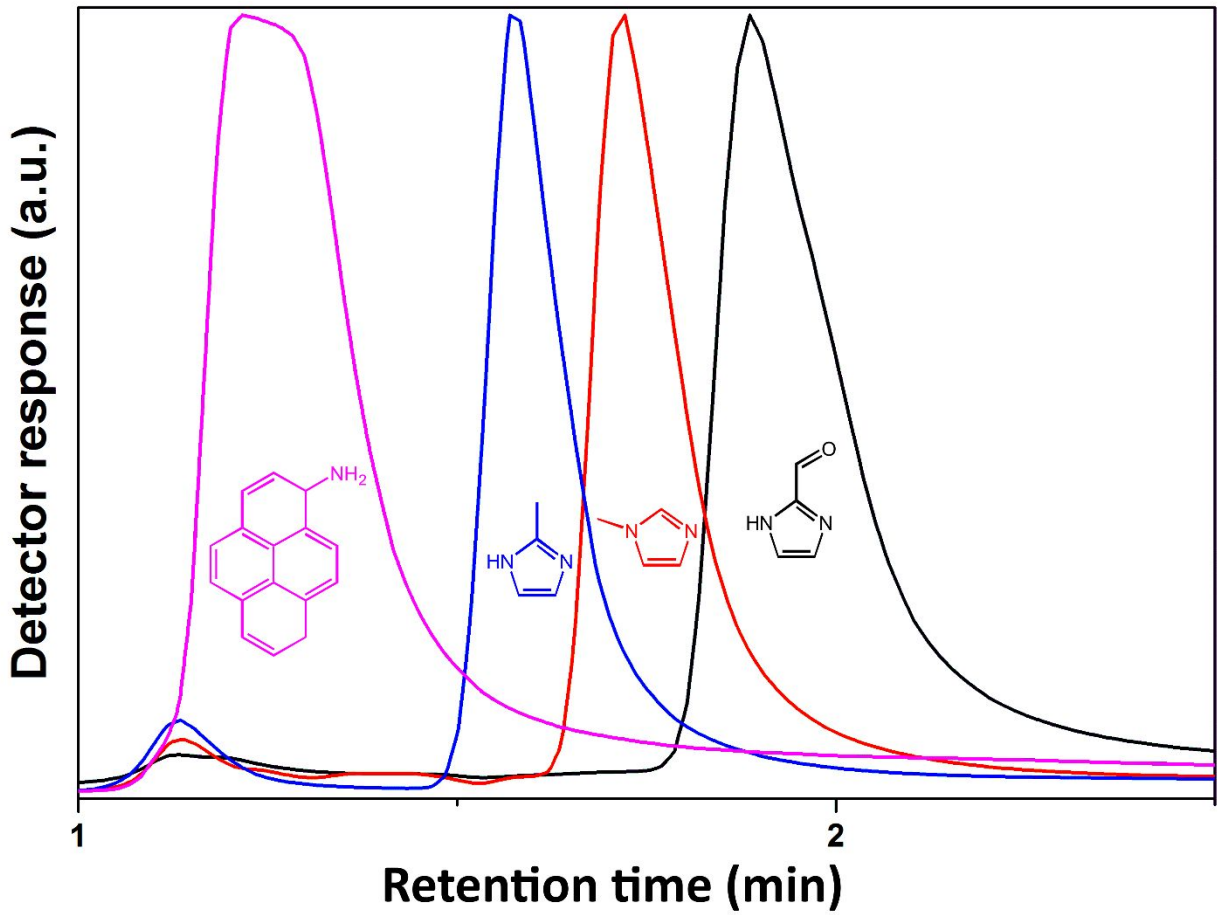

Figure S3_a. Normalized chromatograms with retention times for each of the chemical species of interest.

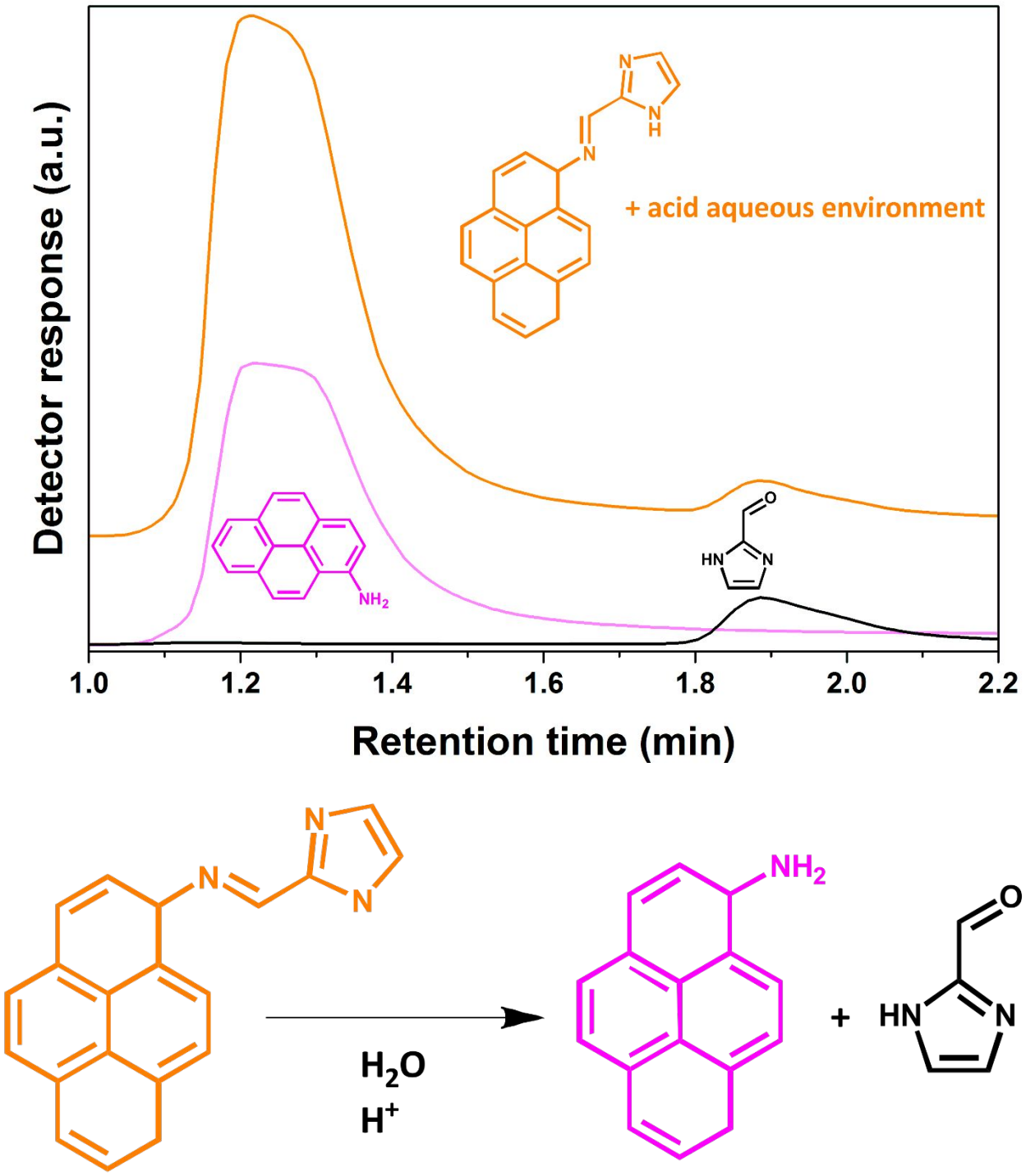

Figure S3_b. Chromatogram for digested Z8S (orange line) superposed to those of 1-aminopyrine (magenta) and 2-imidazolecarboxaldehyde (black). The acidic conditions of the digestion process for the Z8P MOF causes the fluorophore Z8S linkage to hydrolyze into 2-imidazolecaborxialdehyde and 1-aminopyrene.

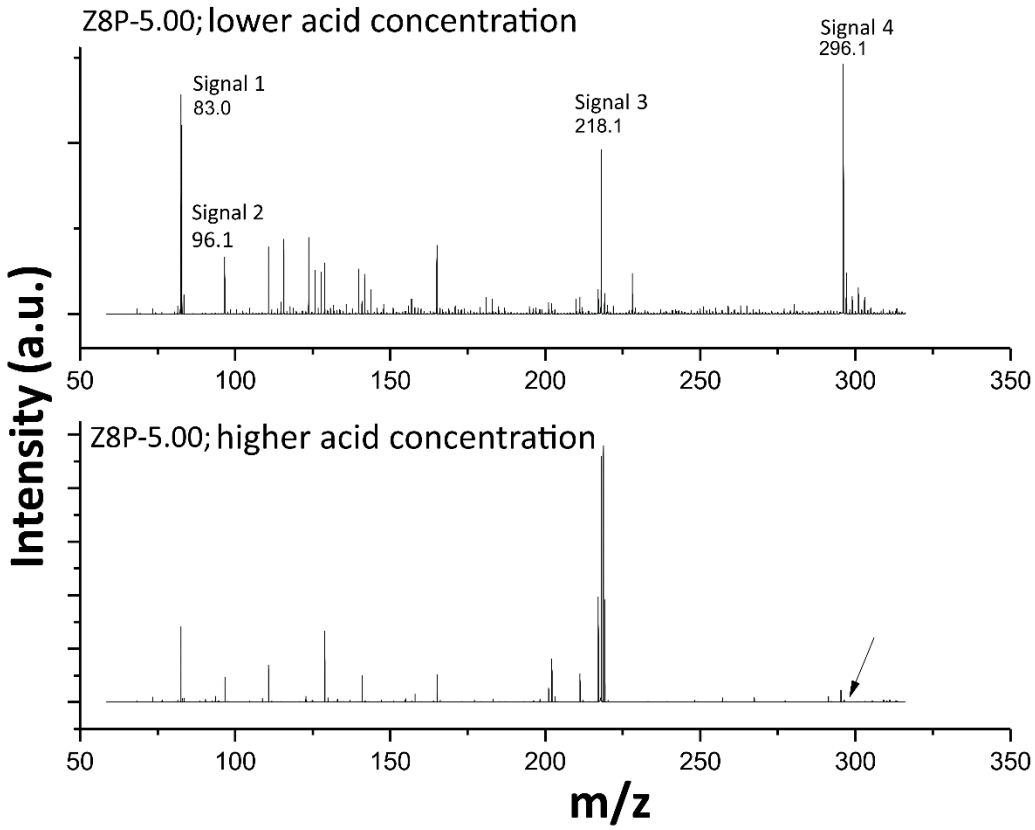

Figure S3_c. Mass spectra for Z8P-5.00 with different volumes of aqueous 1M HCl (top 20 µl [lower acid concentration], pH between 7.0 and 6.3; bottom 50 µl [higher acid concentration], pH under 6.0) on a total digestion volume of 3 ml with 100 mg of Z8P-5.00. On low acidic conditions all species for Z8S can be identified (1- and 2-methylimidazole [Signal 1], 83.0; 2-imidazolecarboxaldehyde [Signal 2], 96.1; 1-aminopyrene [Signal 3], 218,1; Z8P-S [Signal 4], 296,1).

At lower pH, Z8S cannot be identified anymore, and the signals for the aminopyrene, imidazolecarboxaldehyde and 2-methylimidazole intensify. Another effect observed when increasing the share of added 1 M HCl is that many fractions that can be observed on the 120 to the 150 m/z range disappear. We believe these are due to the partial coordination spheres of the zinc with the imidazole species.

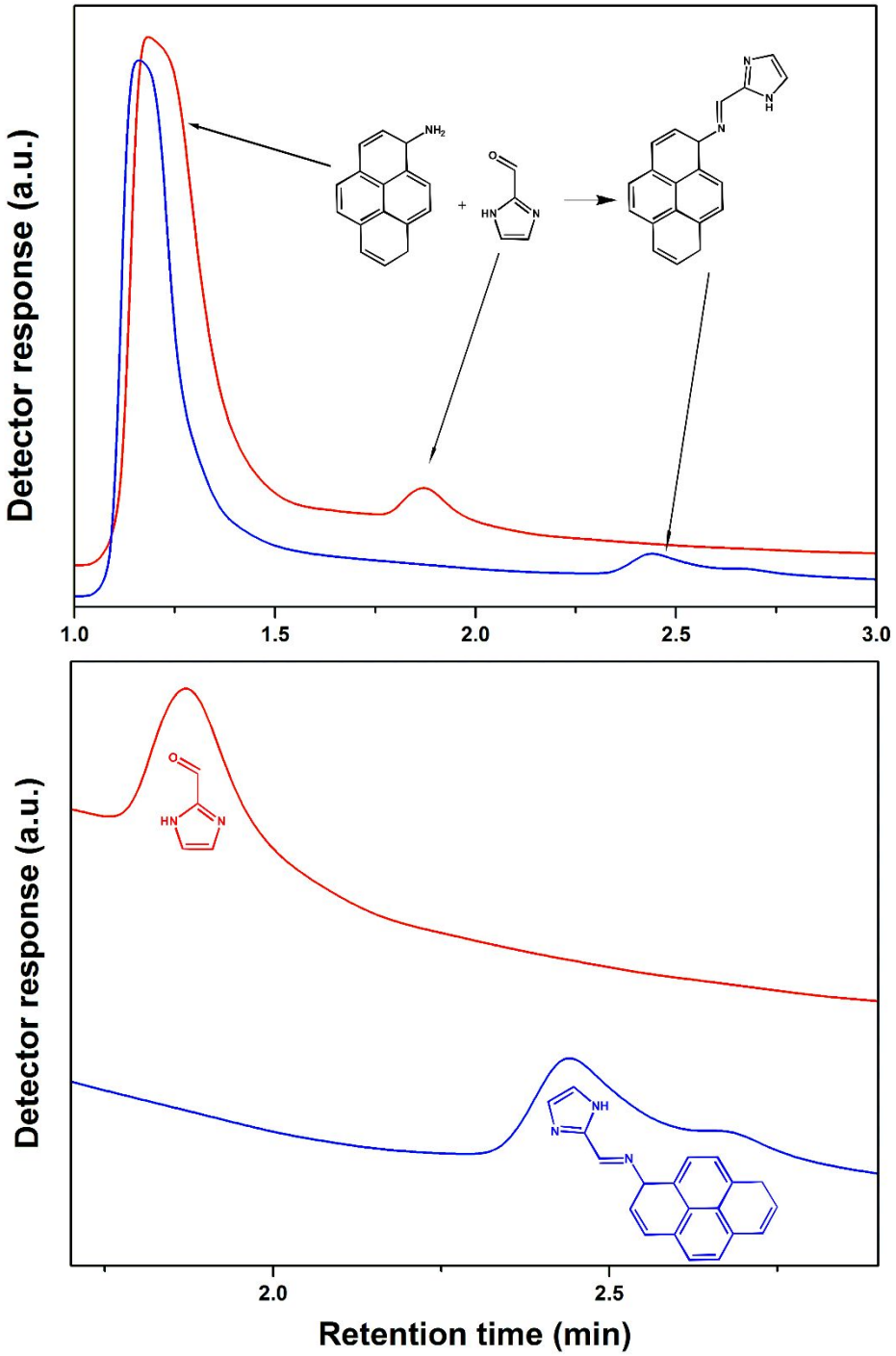

Figure S3_d. HPLC chromatograms of the reaction between 1-aminopyrene and 2-imidazolecarboxaldehyde. The mix was eluted using the eluent with trifluoroacetic acid (TFA, red line) and without TFA (blue line). The results match with the data obtained via mass spectrometry (Figure S3-c). The intensity for the aminopyrine peak suggests that the reaction has a low yield, although it can be also suspected that the acidity of the solid phase on the column was enough to hydrolyze the sensing element (Z8P-S).

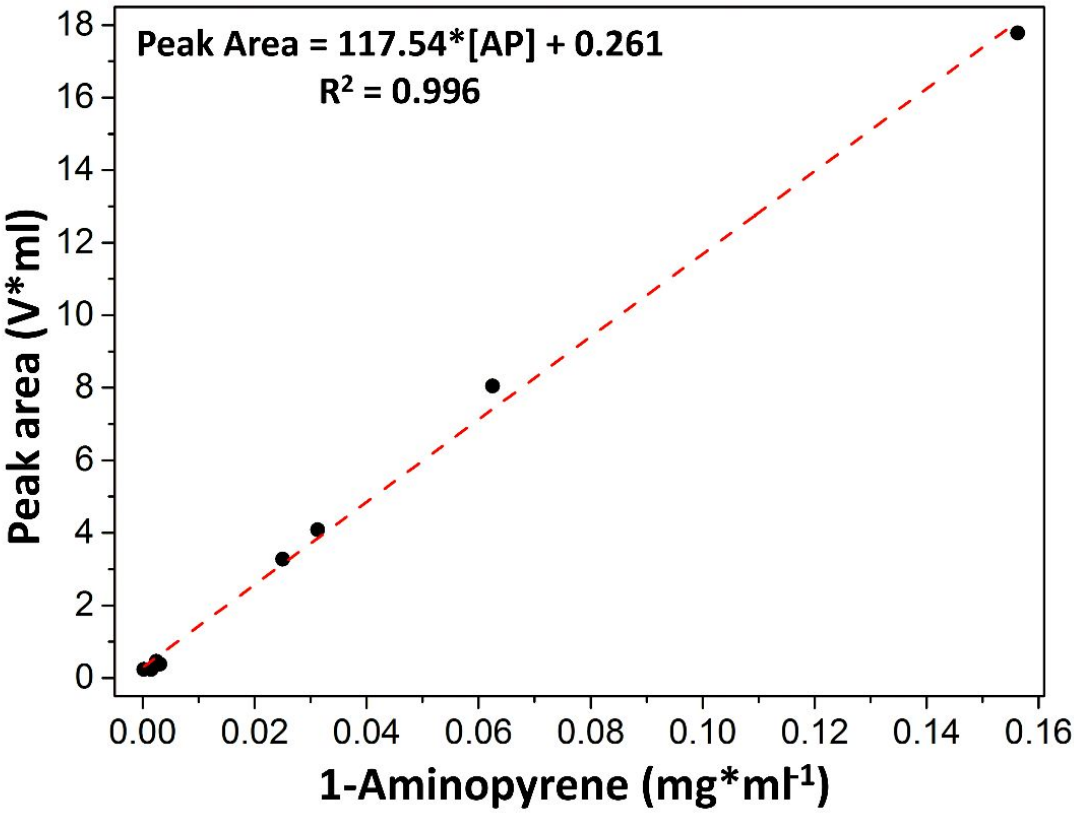
Peak Area = 117.54*[AP] + 0.261
R² = 0.996
Peak area (V*ml)
1-Aminopyrene (mg*ml-1)
0
2
4
6
8
10
12
14
16
18
0.00
0.02
0.04
0.06
0.08
0.10
0.12
0.14
0.16

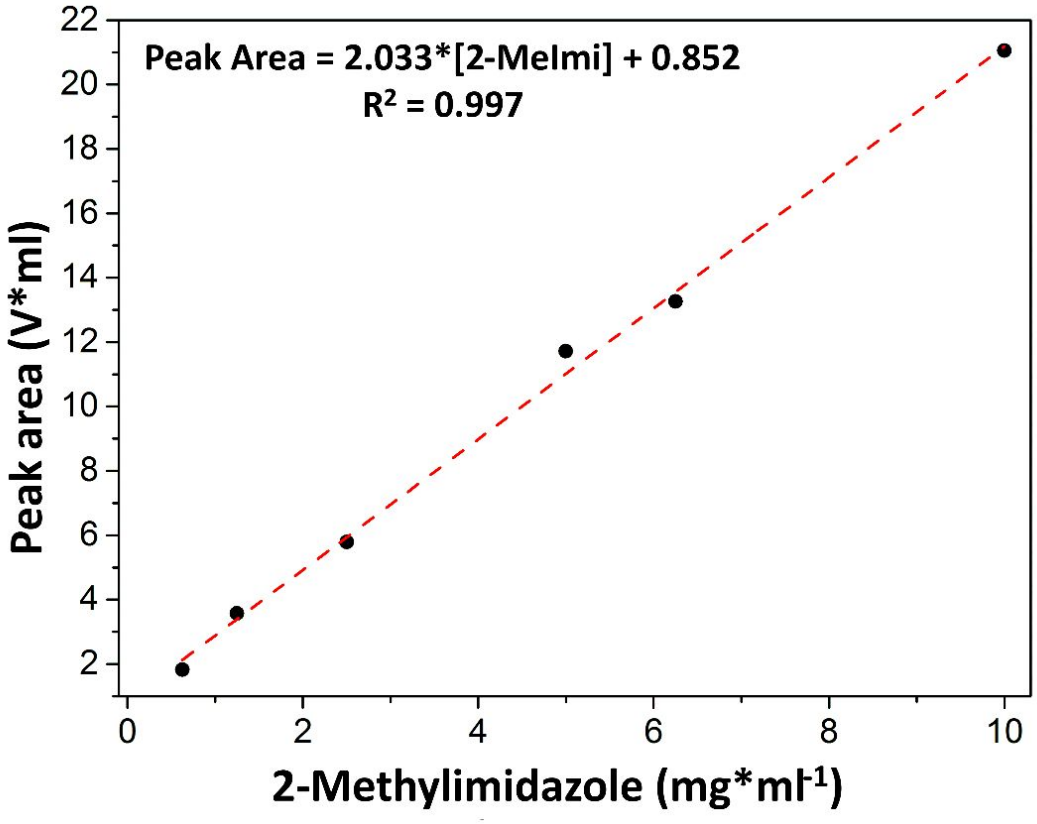
Peak Area = 2.033*[2-MeImi] + 0.852
R² = 0.997
Peak area (V*ml)
2-Methylimidazole (mg*ml-1)
2
4
6
8
10
12
14
16
18
20
22
0
2
4
6
8
10

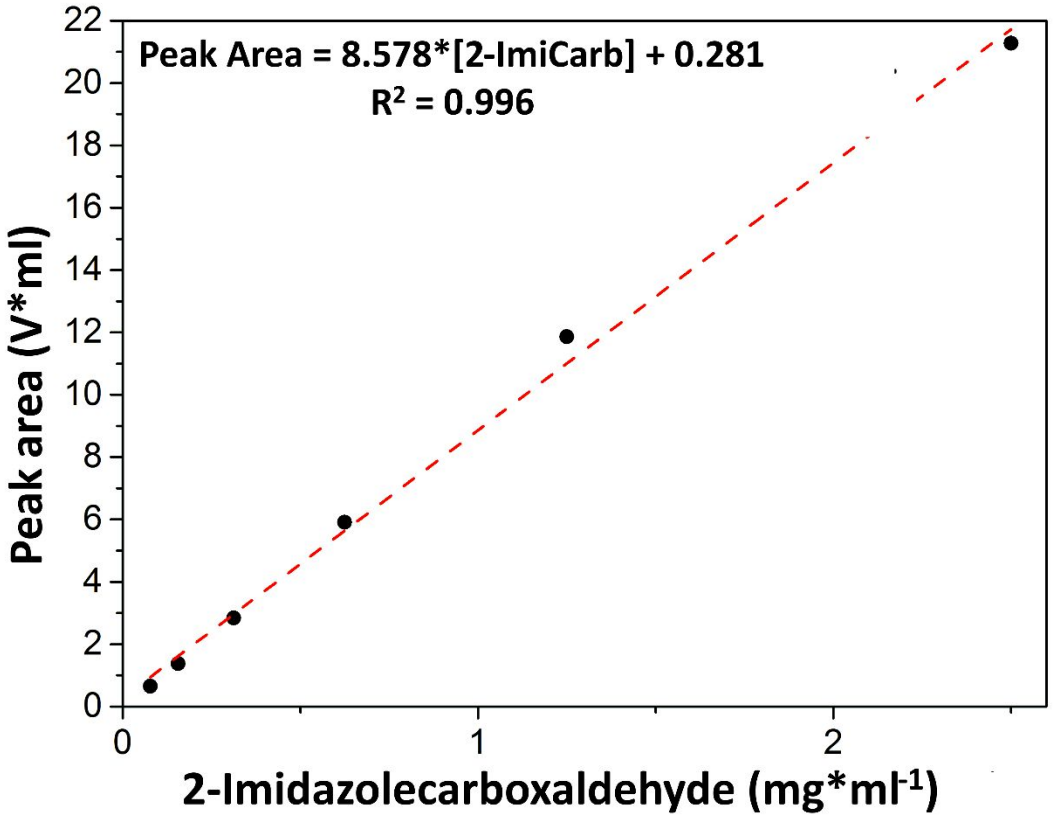

Figure S3_e. HPLC calibration curves for 1-aminopyrine (top), 2-methylimidazole (middle), and 2-imidazolecarboxaldehyde (bottom).

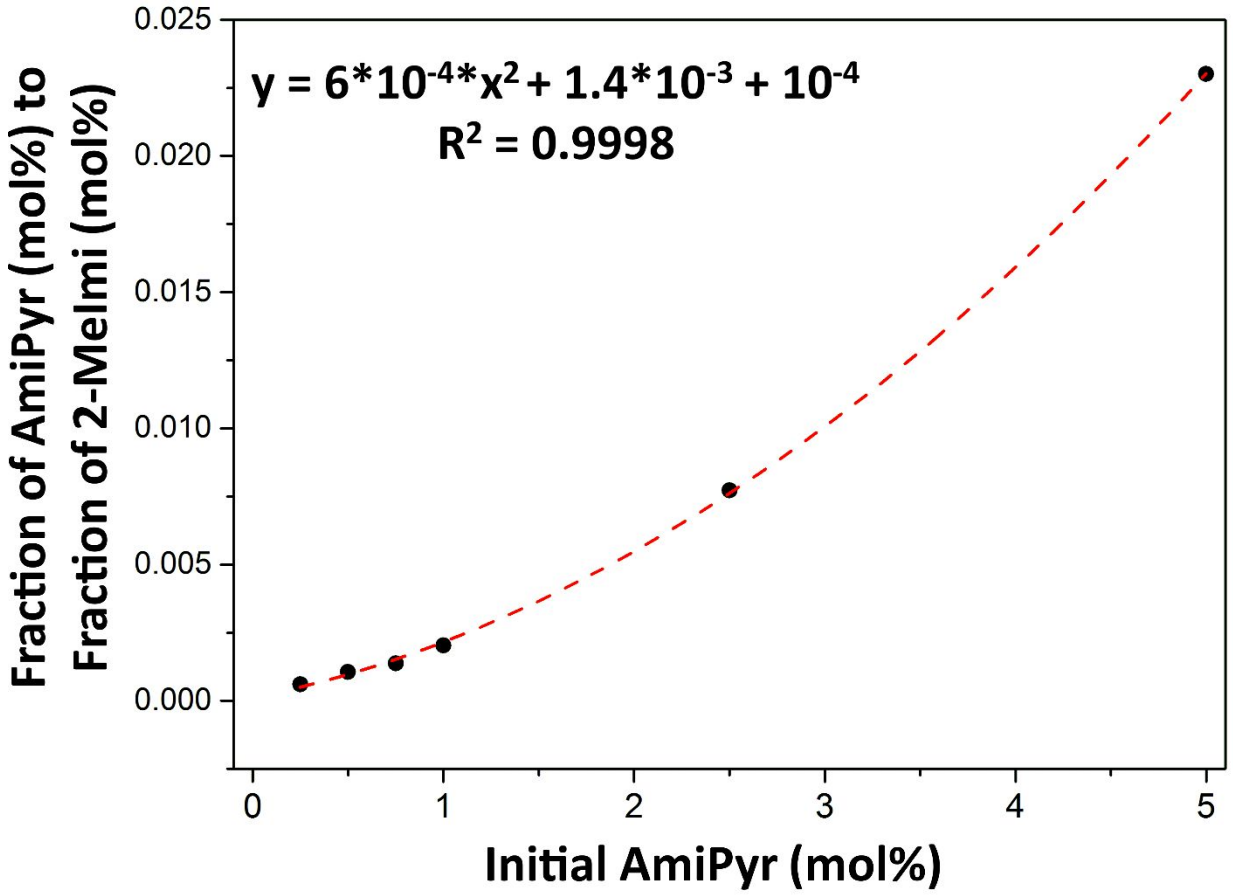

Figure S3_f. Graphical representation of the covalent immobilization of 1-aminopyrene during the synthetic process. The graphic shows the ratio of 1-aminopyrene (in mol%) to 2-methylimidazole (in mol%) in precipitated Z8P MOFs (from Z8P-0.25 to Z8P-5.00) as function of the original concentration for 1-aminopyrene (in mol%) for each Z8P MOF in the mother liquor during synthesis.

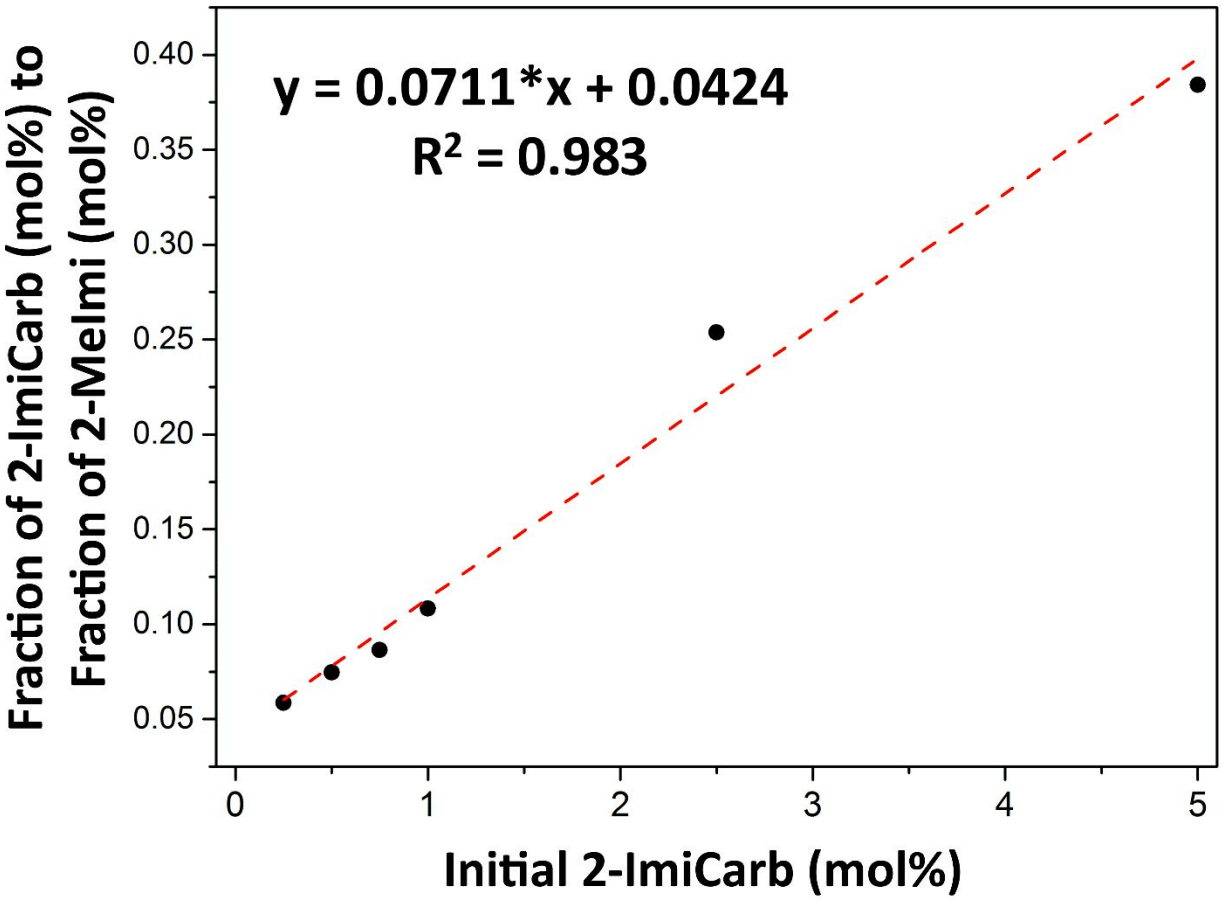

Figure S3_g. Graphical representation of the inclusion of 2-imidazolecarboxaldehyde during the synthetic process. The graphic shows the ratio of 2-imidazolecarboxaldehyde (in mol%) to 2-methylimidazole (in mol%) in precipitated Z8P MOFs (from Z8P-0.25 to Z8P-5.00) as function of the original concentration for 2-imidazolecarboxaldehyde (in mol%) for each Z8P MOF in the mother liquor during synthesis.

Optical Characterization

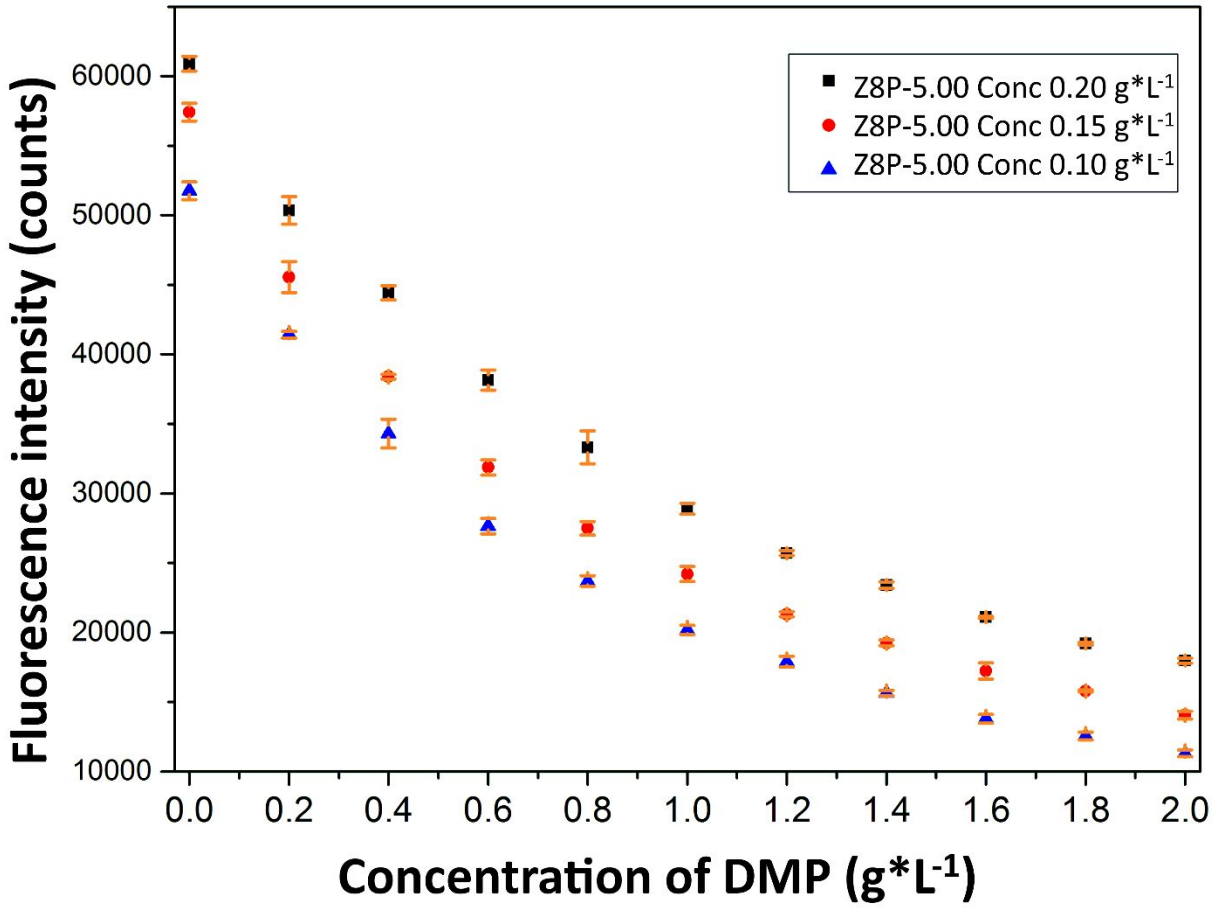

Figure S4_a. Representation of the fluorescence intensity maximum (430 nm) versus the concentration for DMP for three different concentrations for Z8P-5.00 suspended on methanol. The effect of the quenching is independent of the concentration for the sensing element within the investigated range.

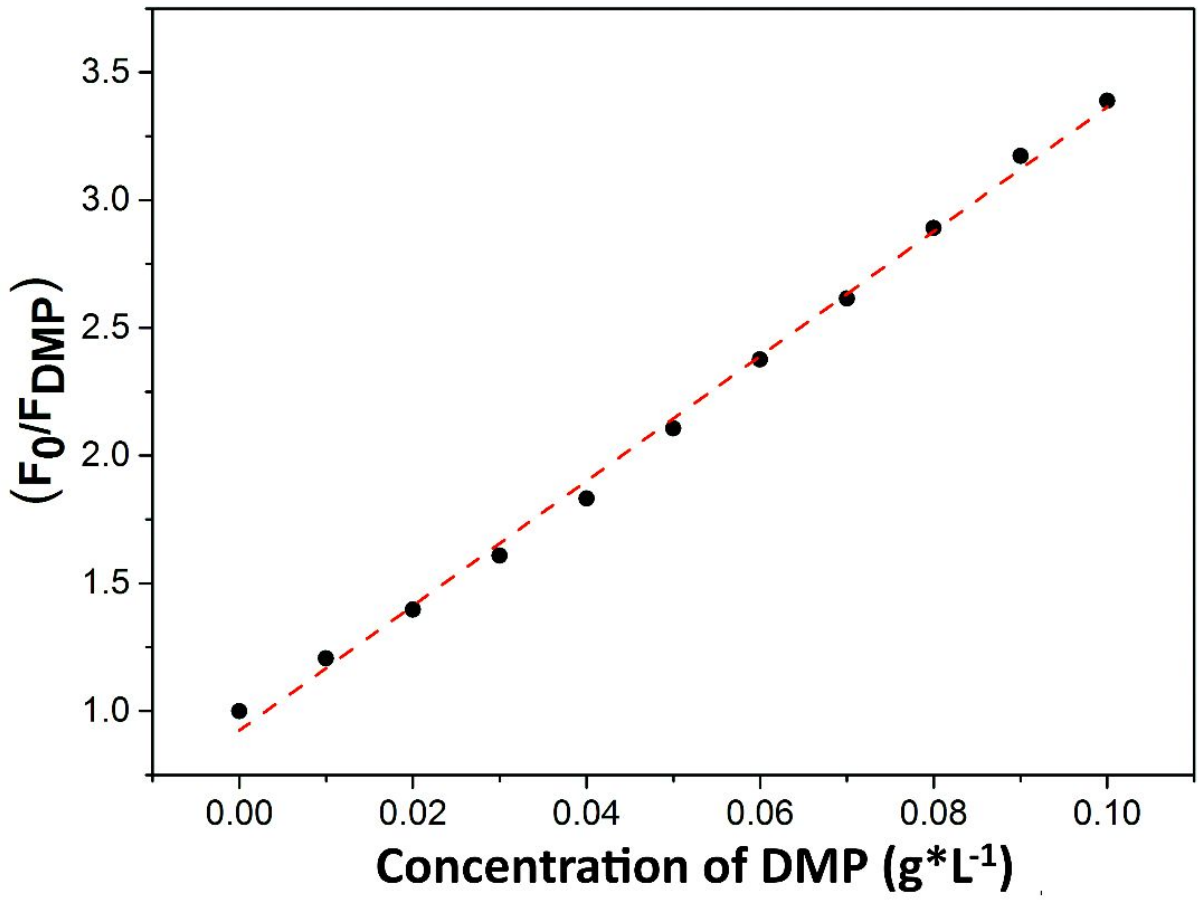

Figure S4_b: Stern-Volmer fitting for the obtained fluorescence data for Z8P-5.00 at the concentration of 0.20 ($g*L^{-1}$) versus changing concentration for DMP. When a linear model was applied the fitting did not suit the obtained data.

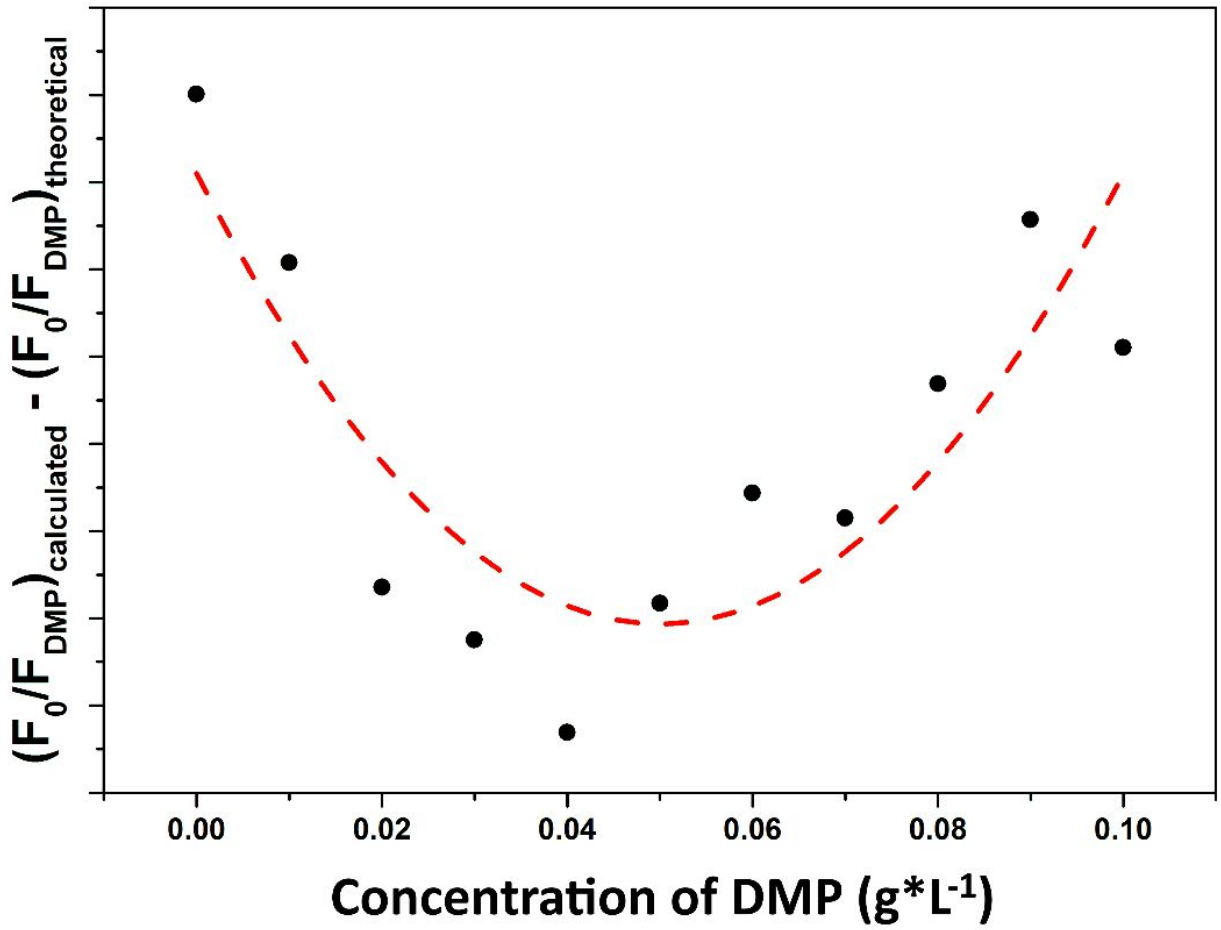

Figure S4_c: Residue curve obtained from subtracting the theoretical fluorescence intensity value from the linear fitting from the real fluorescence intensity values for each DMP concentration. A clear tendency that proves the non-adequacy of the mathematical model applied to the system can be observed. A quadratic mathematical model was then applied to the data that fitted well.

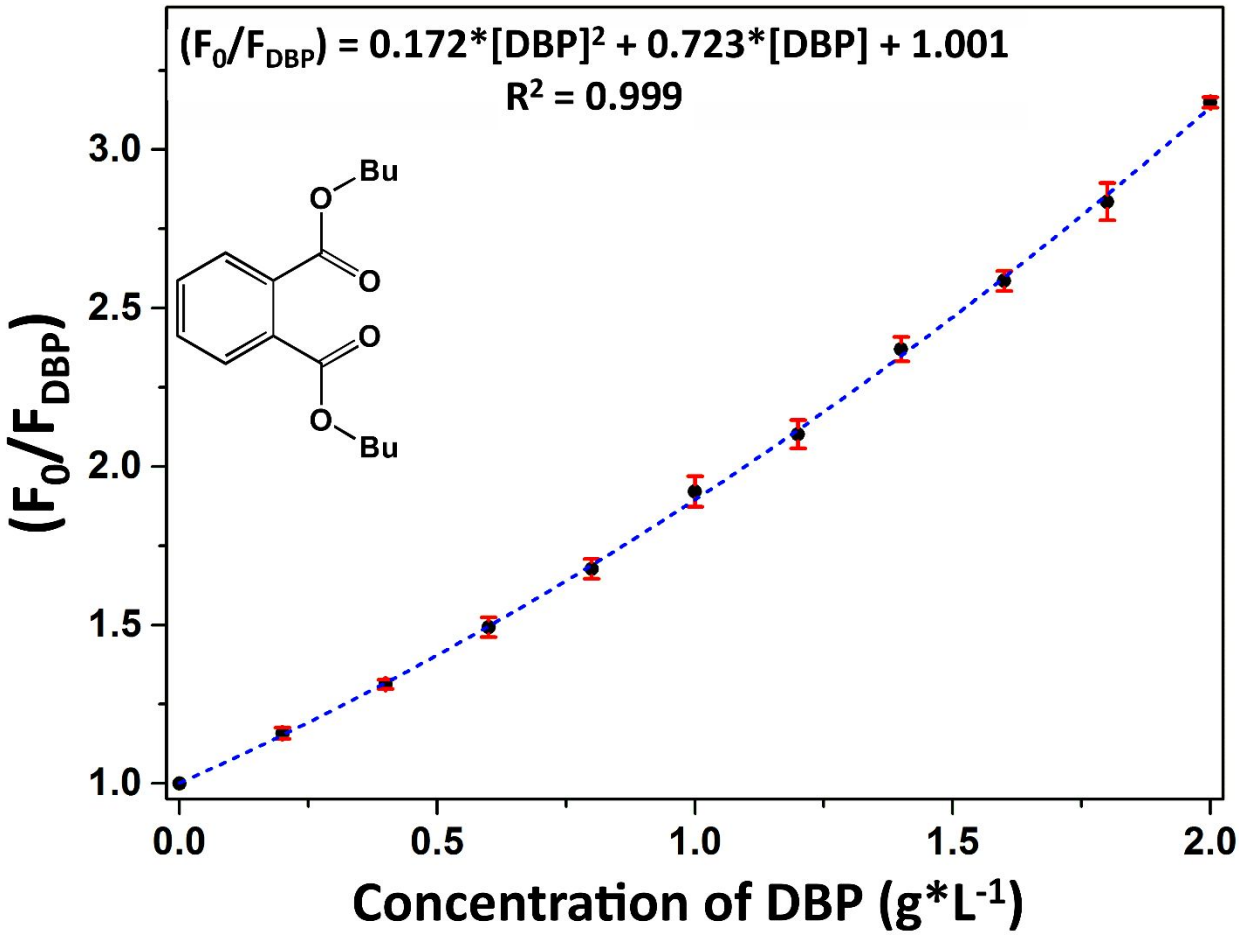

Figure S4_d. Modified Stern-Volmer fitting for the fluorescence quenching of Z8P-5.00 versus di butyl phthalate (DBP) (from 0.0 to 2.0 g*L^{-1}). The excitation wavelength is 277 nm, and the emission is recorded at the maximum at 430 nm.

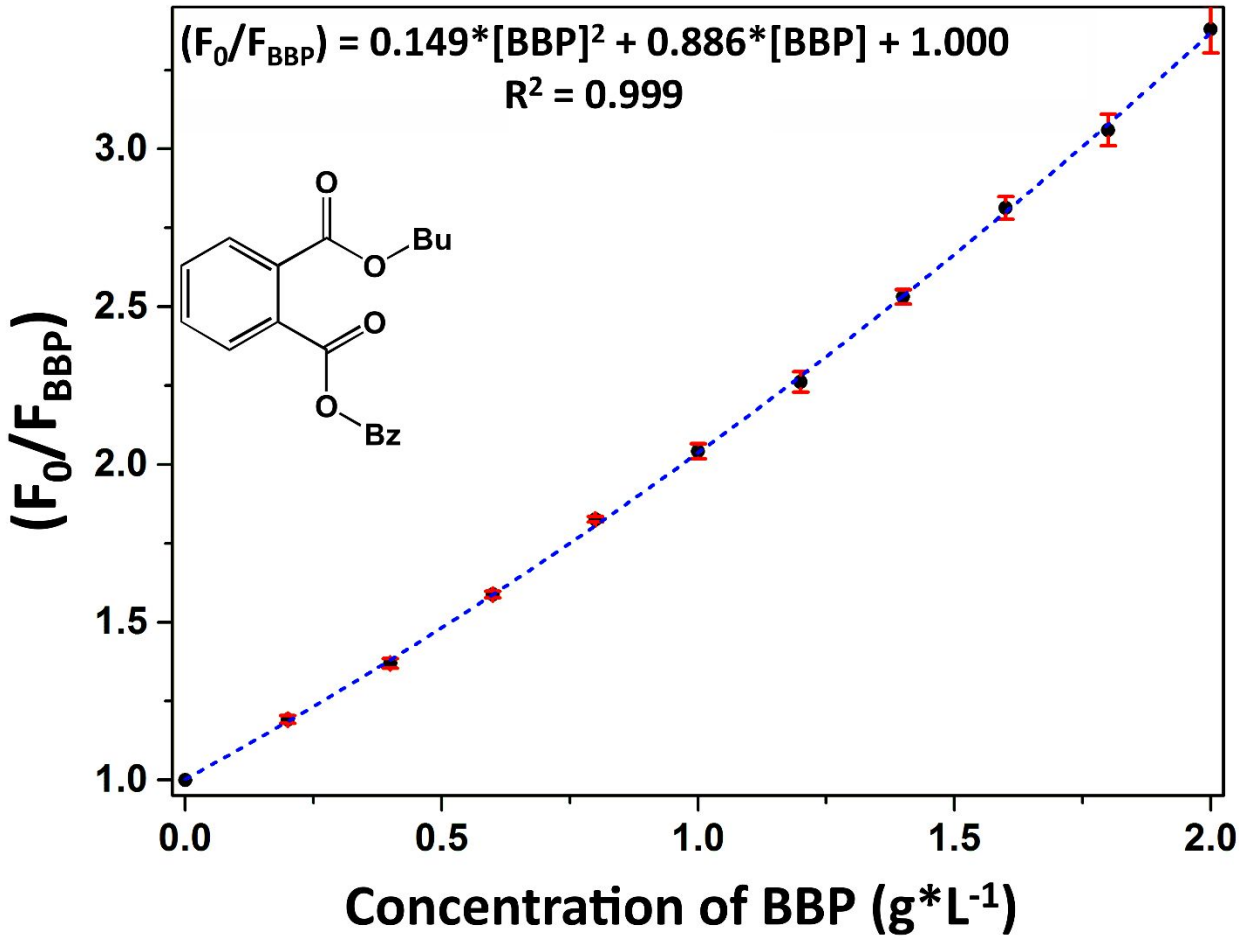

Figure S4_e. Modified Stern-Volmer fitting for the fluorescence quenching of Z8P-5.00 versus benzyl butyl phthalate (BBP) (from 0.0 to 2.0 $g*L^{-1}$). The excitation wavelength is 277 nm, and the emission is recorded at the maximum at 430 nm.

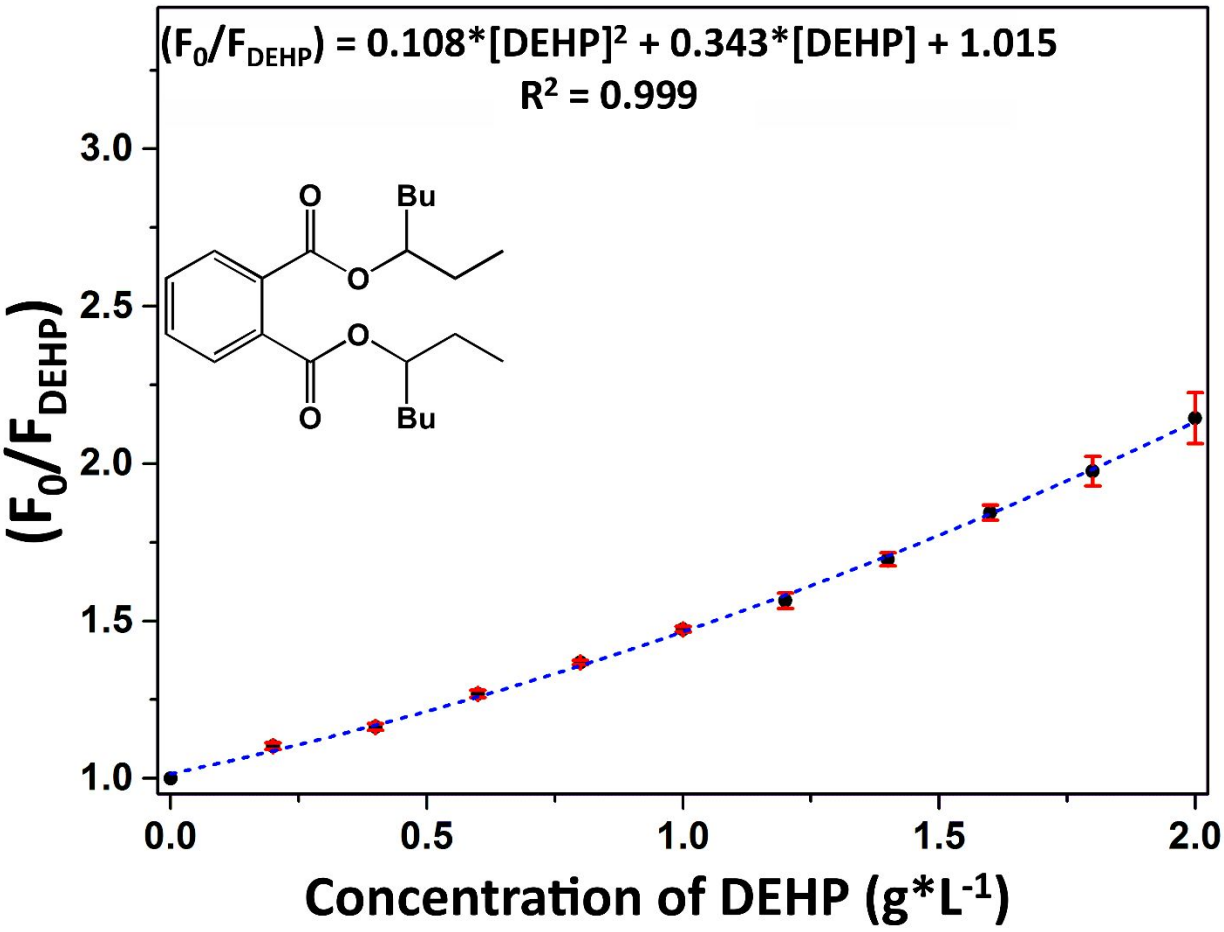

Figure S4_f. Modified Stern-Volmer fitting for the fluorescence quenching of Z8P-5.00 versus di ethyl hexyl phthalate (DEHP) (from 0.0 to 2.0 $g*L^{-1}$). The excitation wavelength is 277 nm, and the emission is recorded at the maximum at 430 nm.

Phthalate analyte	LoD in $g*L^{-1}$
DMP	0.039
DBP	0.026
BBP	0.013
DEHP	0.029

Figure S4_g. Calculated Limits of Detection for the different analytes with the presented system.

Porosity characterization for Z8P-5.00

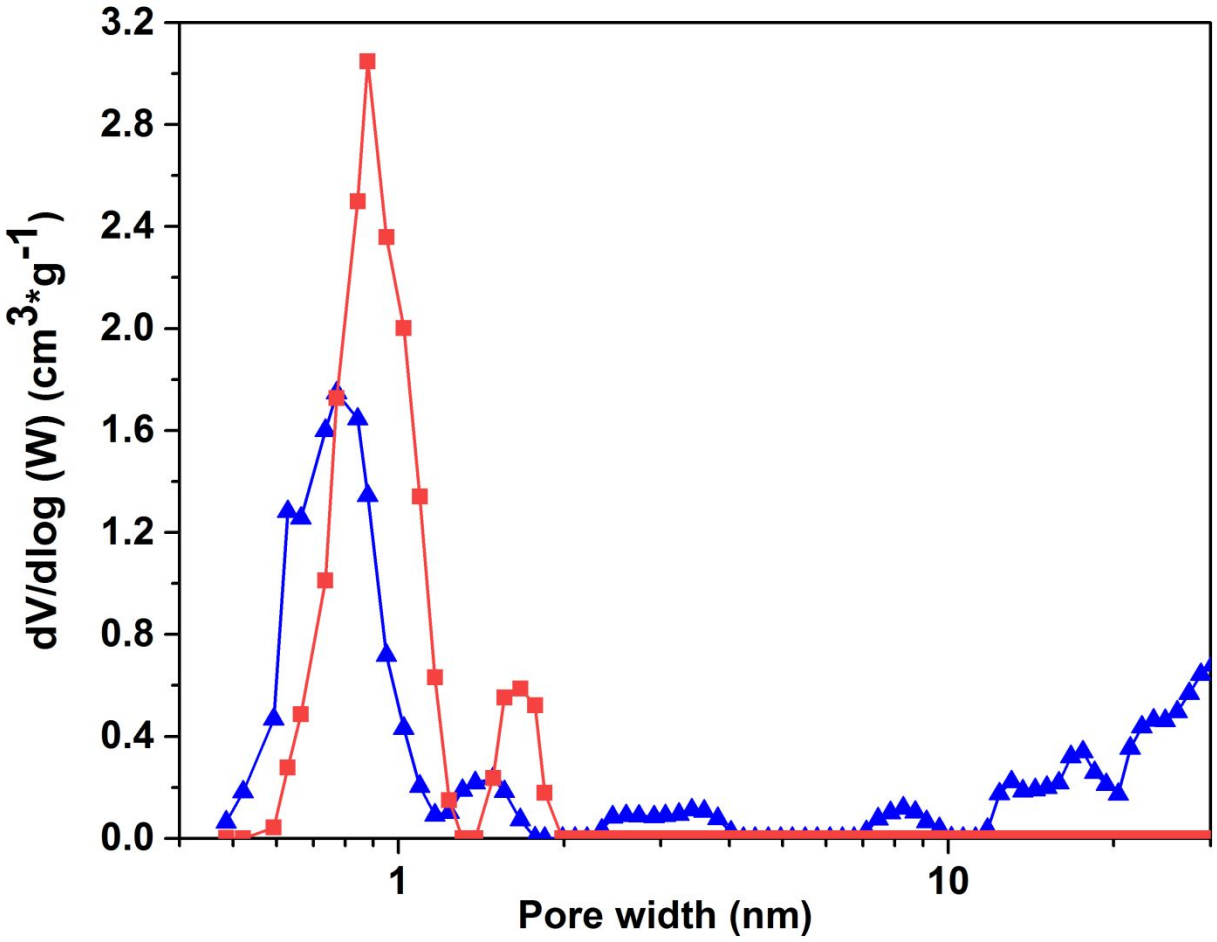

Figure S5_a. PSD for materials ZIF-8 (red squares) and Z8P-5.00 (blue triangles).

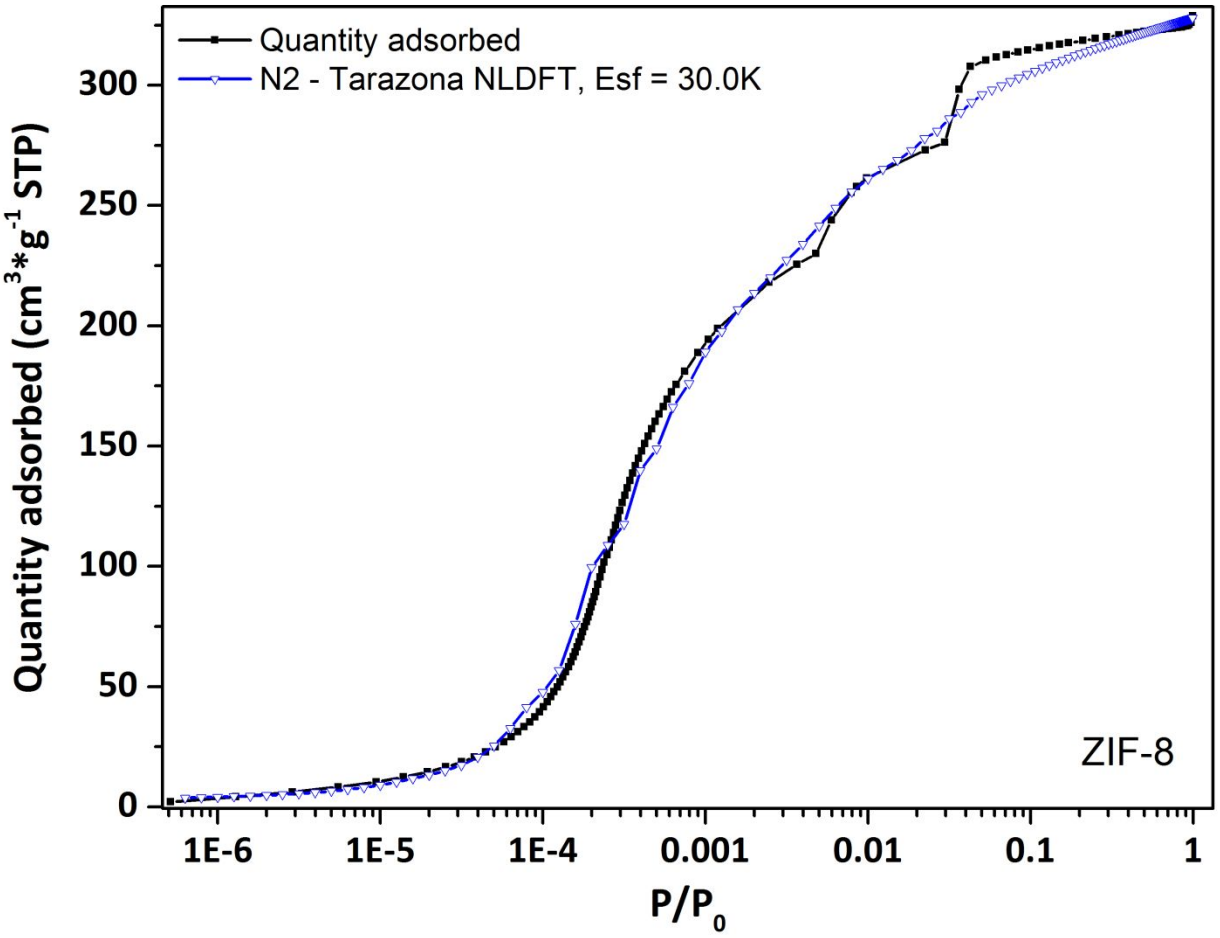

Figure S5_b. N_2 adsorption data at -196°C for material ZIF-8, and calculated values after fitting to NL-DFT.

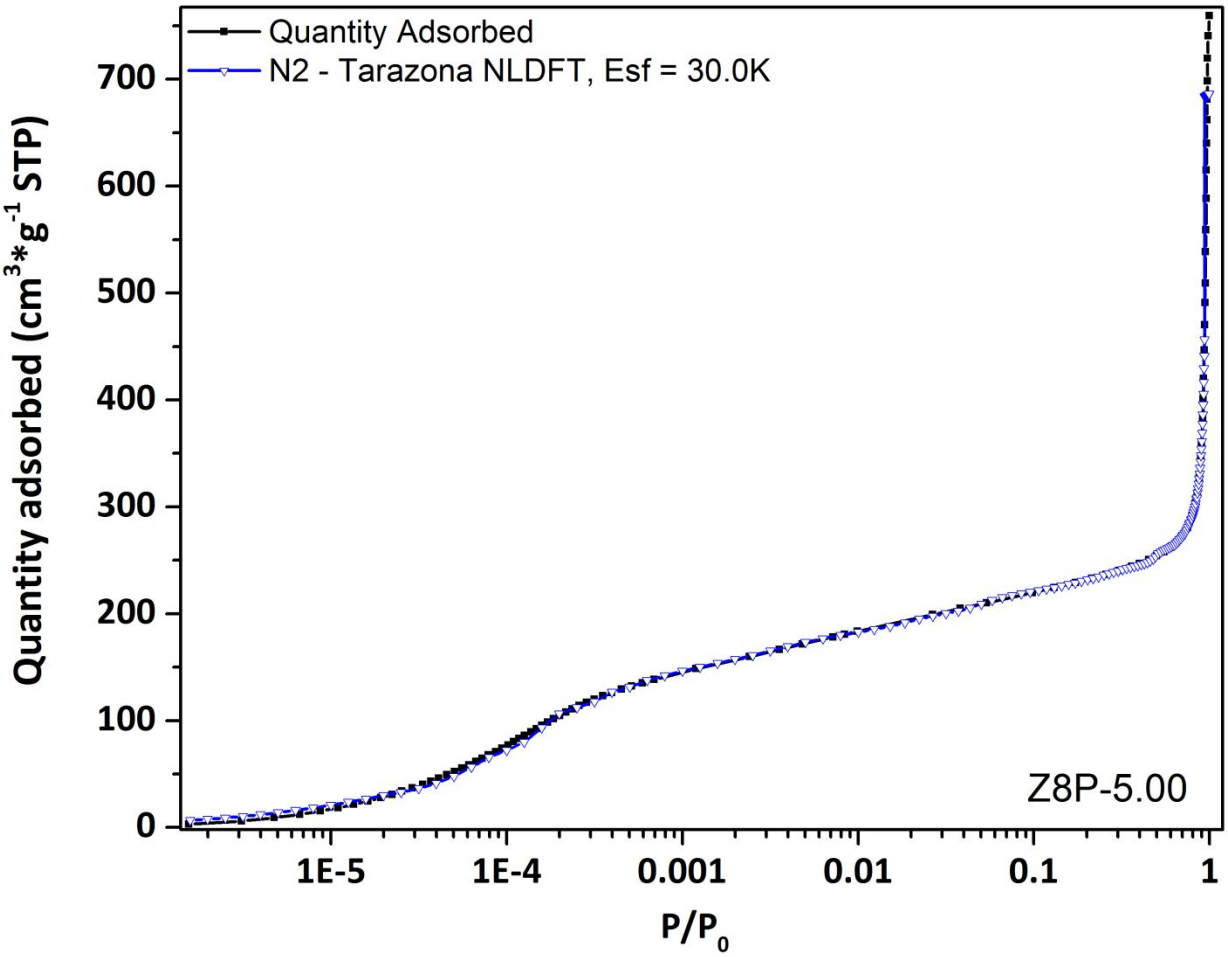

Figure S5_c. N_2 adsorption data at -196°C for material Z8P-5.00, and calculated values after fitting to NL-DFT.